Chain metallicity and competition between paramagnetism and antiferromagnetism in underdoped $YBa_2Cu_3O_{6+x}$: A first principles description

Alessio Filippetti, Giorgia M. Lopez, Mauro Mantega, and Vincenzo Fiorentini
Dipartimento di Fisica and SLACS CNR-INFM, Università di Cagliari, I-09042 Monserrato (CA), Italy
(Received 7 November 2008; published 10 December 2008)

We describe, from advanced first principles calculations, the energetics of oxygen doping and its relation to insulator-metal transitions in underdoped $YBa_2Cu_3O_{6+x}$. We find a strong tendency of doping oxygens to order into nonmagnetic $Cu^{1+}O_x$ chains at any x. Ordering produces one-dimensional metallic bands, while configurations with nonaligned oxygens are insulating. The $Cu^{2+}O_2$ planes remain insulating and antiferromagnetic up to a threshold between $x=0.25$ and 0.5, above which a paramagnetic normal-metal state prevails. The in-plane antiferroparamagnetic competition depends on x but only weakly on the ordering state of the chains.

DOI: 10.1103/PhysRevB.78.233103 PACS number(s): 71.15.Mb, 71.20.−b, 71.30.+h, 74.72.−h

A central puzzle in the physics of the archetypal high-T_c superconducting cuprate $YBa_2Cu_3O_{6+x}$ is the occurrence of several seemingly concurrent phase transitions—structural, magnetic, order-disorder, insulating metal, and superconducting—in the underdoped region of the (T,x) phase diagram. Superconductivity sets on at $x_c \sim 0.35$, so that an insulator-metal transition (IMT) should occur in the CuO_2 planes around the same doping. This IMT, probably associated with a change in magnetic state, is thought be related to an order-disorder transition in the Cu-O chains;[1] holes form a Fermi glass in the low-doping Mott insulator up to a density $h \sim 0.07/CuO_2$ (roughly corresponding to x_c), above which they start percolating in the planes leading to a conventional metal state. Experiments, however, suggest that CuO *chains* undergo an independent IMT at lower doping than the CuO_2 planes. At strong to moderate underdoping ($x \sim 0.2-0.8$), infrared experiments[2] identify the electromagnetic response of the chains as that of a Tomonaga-Luttinger liquidlike one-dimensional conductor, although the chain fragments are too short (~15–400 Å) to support dc across macroscopic regions [except for weak underdoping ($x=0.95$) whereby they are conducting[3,4]]. Optical data[5] show that oxygens cluster in metallic islands with local orthorhombic symmetry even at minute doping and that metallic percolation through the chains occurs at a doping as low as $x=0.1-0.2$.

It is fair to say that the relation of chain ordering with one-dimensional metallization and with the IMT in the CuO_2 planes at higher doping has never been described thoroughly from first principles. Here, using advanced first principles electronic structure calculations, we (a) study the connection between intrachain one-dimensional metallicity and oxygen ordering in (nonmagnetic) CuO chains as a function of doping and (b) analyze the competition of the antiferromagnetic (AF) insulating and paramagnetic (PM) metallic states of the CuO_2 planes in different chain ordering configurations. The picture we arrive at is as follows. $YBa_2Cu_3O_6$ is, as expected, a Mott-Hubbard insulator. At small x it remains everywhere insulating inasmuch as doping oxygens are disorderly distributed through the chains. A dispersed one-dimensional metallic band appears when oxygens orderly align into CuO chains. Chain alignment is found to be always favored, consistently with the evidence that chain nucleation starts immediately at $x>0$ and that metallic percolation in the chains is already detectable at $x \sim 0.1$.[2,5] The dispersed band has a strongly dominant chain-atom character, and holes remain largely bound to the doping oxygen O(1) and the nearby Cu(1) ions. Only a minor hole fraction is transferred to the CuO_2 planes (indicating a rather sharp decoupling of the two playgrounds): the ensuing small variations in orbital occupations govern the very tight competition between the in-plane insulating AF state and the conventional metallic PM phase. The AF state gives way to the PM metallic state at a doping between $x=0.25$ and 0.5, consistent with the overall metallization threshold implied by the superconductive onset; intriguingly, this crossover occurs *independently* of the way O(1)'s are distributed in the chains, i.e., on the order-disorder interplay governing the in-chain IMT.

The realistic description of underdoped cuprates is troublesome for first principles band theories such as local-spin-density approximation (LSDA) or generalized gradient approximation (GGA) density-functional theory,[6] which incorrectly describe the antiferromagnetic Mott insulating state as nonmagnetic and metallic and therefore are not usable to study the IMT. Here we circumvent this issue employing the pseudo-self-interaction correction (PSIC) method,[7] which is particularly accurate for strongly correlated materials.[8] As a

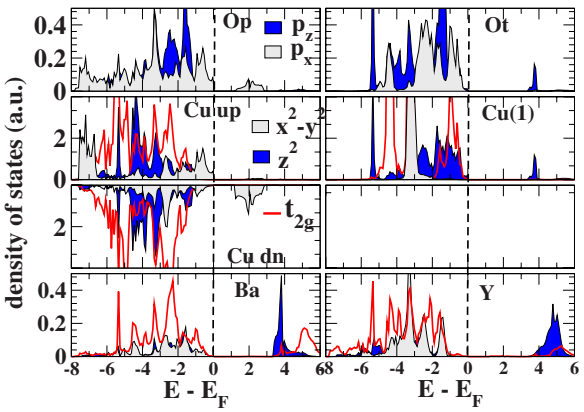

FIG. 1. (Color online) OR-DOS of AF $YBa_2Cu_3O_6$. O(2) and O(4) are in-plane and apical oxygens, respectively. Only the most important orbitals (d for Cu, Ba, and Y and p for O) are shown; the solid (red) line is sum of the three nearly degenerate t_{2g} DOSs. For O_P $p_y \sim p_z$, while for O_T $p_x=p_y$. Supercell: 48 2×2 atoms.

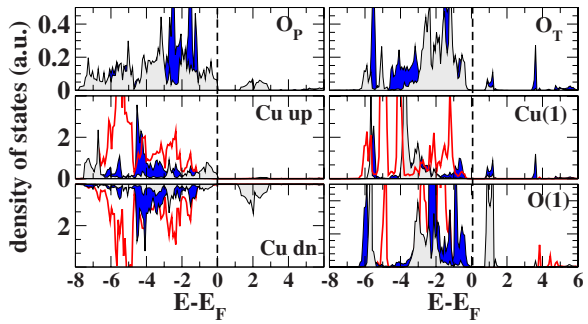

FIG. 2. (Color online) OR-DOS of AF $YBa_2Cu_3O_{6.25}$ for the broken-chain configuration (a) in Fig. 3. Labels are the same as Fig. 1.

backup and countercheck, we also use GGA+U (Ref. 9) and GGA calculations. PSIC calculations are carried out with a plane-wave basis ultrasoft pseudopotential[10] method, with 30 Ry cutoff energies. For GGA and GGA+U we employ the projected augmented wave (PAW) method as implemented in the VASP (Ref. 11) code. We use $6\times6\times6$ special k-point grids for total-energy calculations and 250 special k points and linear tetrahedron interpolation for density of states (DOS). The GGA+U parameters $U=10$ eV and $J=1$ eV, give the best match with PSIC bands. At different doping concentrations, we use supercells ranging from 24 ($\sqrt{2}\times\sqrt{2}\times1$ primitive cells) up to 96 atoms ($4\times2\times1$). Unless otherwise specified, the results shown below are obtained by PSIC.

In Fig. 1 we show the orbital-resolved (OR)-DOS) for tetragonal AF $YBa_2Cu_3O_6$, which shows a Mott-Hubbard charge-transfer band gap of 1.2 eV [the observed photoconductive threshold is at 1.5 eV (Ref. 1)]. The valence-band top (VBT) and conduction-band bottom (CBB) are hybrids of unpolarized O (p_x,p_y) and, respectively, majority (occupied) and minority (unoccupied) Cu $d_{x^2-y^2}$ states. The fundamental transition only involves orbitals within CuO_2 planes; transitions involving final states with apical O(4) p_z and chain Cu(1) d_{z^2} states (as well as Ba and Y states) start only above ~3.5 eV (more details will be presented elsewhere).

Now we consider oxygen inclusion in the chains. In Fig. 2 we show the OR-DOS at $x=0.25$ calculated with one doping oxygen per 2×2 unit cell [configuration (a) of Fig. 3] corresponding to an alternated array of parallel isolated Cu(1)-

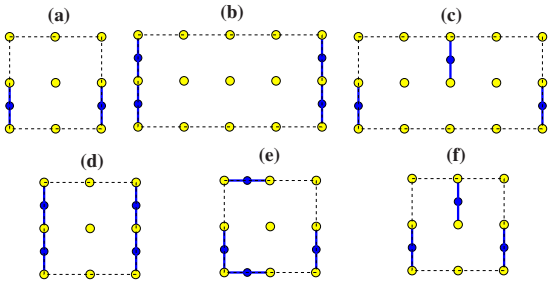

FIG. 3. (Color online) Doping configurations in the Cu(1)-O chains. Dark (blue) and light (yellow) circles are O(1) and Cu(1) ions, respectively. (a) $x=0.25$, cell 2×2; [(b) and (c)] $x=0.25$, cell 4×2; and [(d)–(f)] $x=0.5$, cell 2×2.

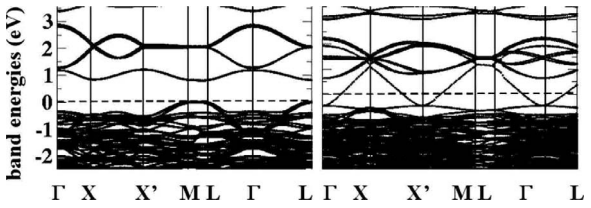

FIG. 4. Band structure of AF $YBa_2Cu_3O_{6.25}$. Left: broken chain [configuration (a) of Fig. 3]. Right: full chains [configuration (b), same figure].

O(1)-Cu(1) segments: this is our broken-chain configuration. The main feature induced by O(1) is a spin-degenerate hole state at ~1 eV above the VBT, strongly localized on O(1) itself with dominant p_x character [x is the Cu(1)-O(1) direction]. This hole is residually extended (Fig. 2) on Cu(1) $d_{x^2-y^2}$ (through dominant $pd\sigma$ coupling) and, more conspicuously, on Cu(1) d_{z^2}. This is because d_{z^2} is the highest (most antibonding) Cu(1) d state [see Cu(1) OR-DOS in Fig. 1]. The hole further propagates to apical O(4) p_z states (see Fig. 2) and up into the CuO_2 planes. The calculated orbital decomposition of the hole band gives 32.3% on O(1), 33.5% on the two adjacent Cu(1), 27% on the apical O(4) closer to the latter, 2.5% on O(2), 1.3% on Cu(2), and finally 2.3% on Ba. The corresponding band structure (left panel of Fig. 4) shows the flat hole band running through the whole Brillouin zone just below the undoped conduction band (actually almost touching it at Γ).

To evaluate the effects of oxygen alignment at $x=0.25$ [configuration (b) of Fig. 3] we employed a 4×2 (i.e., 98-atom) supercell, whose band structure is reported in the right panel of Fig. 4. Now the hole band is dispersed and crosses the Fermi energy, so the system is metallic. The dispersion is one-dimensional; no metallicity is injected into the CuO_2 layer, as signaled by the band flatness along the M-L k_z segment. Even at $x=0.5$ the OR-DOS of the chain-ordered AF configuration (Fig. 5) shows that the hole band does not affect the band gap in the AF CuO_2 layer and spreads instead on the same in-chain orbitals previously seen to be involved in the localized hole decomposition.

So far we have shown that the order-disorder and one-dimensional IMT in the chains are directly related. This re-

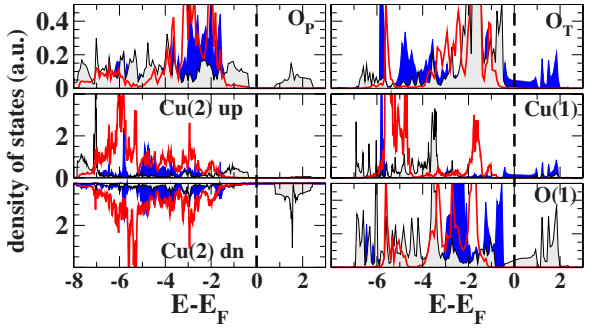

FIG. 5. (Color online) OR-DOS of ordered-chain AF $YBa_2Cu_3O_{6.5}$. The calculation is done in configuration (d) of Fig. 3. Labels are same as in Fig. 1. Note that while dispersed band crossing E_F has sizable Cu(1)-O(1)-O(4) character, the local DOS in the CuO_2 planes is still insulating.

TABLE I. Total energies for the O(1) configurations in Fig. 3 [(b) and (c)] for $x=0.25$ and [(d)–(f)] for $x=0.5$ and AF and PM phases (values labeled with * and ** refer to GGA+U and GGA calculations, respectively).

	$x=0.25$		$x=0.5$		
	(b)	(c)	(d)	(e)	(f)
ΔE^{PM}	0	1.06 (0.80*, 0.69**)	0	0.78	1.08
ΔE^{AF}	0	1.07 (0.98*)	0	0.82	1.12

lation holds for $x=0.25$ and $x=0.5$, so it must hold for any $0.25<x<0.5$. Of course the modeling of disorder in our calculations is limited by supercell size; for a realistic sample of disordered distributions we may envisage a hole energy distribution gradually spanning (and eventually closing) the ~ 1 eV energy interval above the VBT. So, rather than as an optical insulator, the chain electronic ground state is probably better described as a hopping-conductive Fermi glass, in agreement with the mainstream interpretation. However, the limits in simulating disorder effects do not change the conclusion that (a) only chain alignment produces hole band dispersion, (b) the hole band is one-dimensional in character, and the corollary that (c) as long as the AF ordering is retained, metallic conductivity is not transferred outside the chains.

We now discuss the energetics of chain-aligned and unaligned configurations at $x=0.25$ and $x=0.5$. The data for both AF and PM orderings, obtained with different approaches, are listed in Table I. The chain-ordered configuration is the most stable by a safe margin, irrespective of CuO_2 magnetic ordering. Thus ΔE can be thought of as the cost of breaking a single chain moving an O(1) to the nearby isolated segment. These results imply a strong drive toward chain formation and hence one-dimensional metallic behavior. Although disorder does not allow the formation of macroscopic chains at low doping,[2] our calculated energies confirm the observation that chain nucleation starts at very low doping, also accompanied by local one-dimensional metallic percolation.

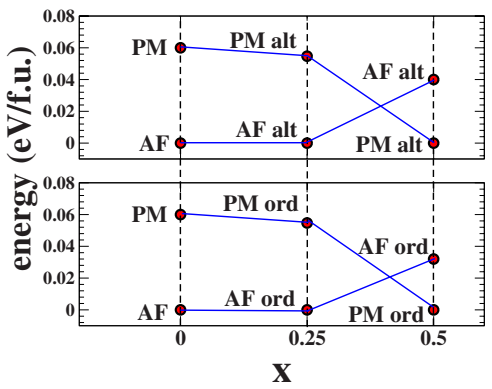

FIG. 6. (Color online) Comparison of the energies of AF and PM phases as a function of x for broken-chain (top) and ordered-chain (bottom) configurations. For $x>0$ the energy zero in the upper panel is about 1 eV higher than in the lower panel (see Table I).

TABLE II. Differences (in 10^{-3} unit charge) in atomic-orbital occupation between $x=0$ and $x=0.5$ for PM and AF orderings and chain configurations (d) and (f) (see Fig. 3). Positive (negative) charges are hole (electron) fractions. The number of equivalent atoms in the cell is in square brackets. Subscript "1" indicates atoms next neighbors of O(1) or in apical units containing O(1); subscript "2" non-neighbors of, or in units without, O(1): e.g., $O(4)_1$ is first neighbor to a Cu(1)-O(1) unit; $O(2)_1$ is on top of O(1), $O(2)_2$ and $O(2)_3$ are coplanar to $O(2)_1$; $Cu(1)_1$ and $Cu(1)_2$ are first or second neighbors of O(1); and $Cu(2)_1$ and $Cu(2)_2$ are on top of $Cu(1)_1$ and $Cu(1)_2$, respectively.

	PM_d	AF_d	PM_f	AF_f
Doping				
O(1) [2]	−403	−401	−364	−361
Total O(1)	−806	−802	−728	−722
Apical				
$O(4)_1$ [4]	65	67	34	35
$O(4)_2$ [4]	1	11	34	35
$Cu(1)_1$ [2]	189	190	103	105
$Cu(1)_2$ [2]	35	36	103	105
CuO_2 [4]	187	191	170	174
Total Cu(1)	448	451	413	418
Total Cu(1)+O(4)	747	764	682	697
Planar				
$O(2)_1$ [4]	3	10	2	7
$O(2)_2$ [4]	−2	3	−2	3
$O(2)_3$ [8]	2	7	1	5
Total O(2)	23	106	10	82
$Cu(2)_1$ [4]	13	−4	10	−4
$Cu(2)_2$ [4]	11	−5	10	4
CuO_2 [8]	15	9	11	6
Total Cu(2)	98	−34	77	−34
Total Cu(2)+O(2)	121	72	86	48
Y [4]	−3	0	−3	0
Ba [8]	−4	−1	−2	0

Next, in Fig. 6 we compare the AF and PM total energies for chain-ordered [(b) or (d)] and chain-alternated [(c) or (f)] configurations as a function of x. The zero energy is the lowest phase at each doping. The AF phase is favored up to $x=0.25$ whereas the PM phase is favored at and above $x=0.5$.

Three points are worth noticing. First, the AF→PM crossover (with attendant in-plane insulating→metallic transition) occurs in the doping interval where superconductivity sets on. Second, the AF-PM competition is barely affected by the O(1) distribution within the chains; this implies in both instances a weak chain-plane coupling with minimal hole transfer to the planes, confirming the high inefficiency of oxygen doping. Third, the AF-PM competition is quite tight (a few tenths of meV/f.u.), in line with the tendency of the AF phase to form cluster spin-glass states and the coexistence of microscopic AF and PM domains.[12]

The AF-PM competition can be interpreted analyzing the changes in orbital occupation upon doping, reported in Table II. Each O(1) takes over ~0.4 electron. This quantity is quite independent of magnetic ordering but visibly larger for configuration (d) than for (f); full-chain order enhances charge transfer between the doping O and its surrounding. The vast majority of the hole released by O(1) remains in the apical units [Cu(1)-O(1)-O(4)], and only a fraction is transferred to the planes. The most receptive environment is PM_d, which collects 13.9% of the hole charge into the planes, followed by PM_f (11.2%), AF_d (8.7%), and AF_f (6.4%).

We can understand this classification in terms of magnetic and chain ordering. The PM phases have in-plane CuO_2 bands at E_F, allowing hole injection in the highly receptive Cu(2) atoms. In AF phases the Cu(2) states are swept off the E_F region and are marginally affected by hole injection. Table II shows that the PM in-plane hole population is mainly on Cu(2), while in the AF phase in-plane holes mainly reside on O(2), with Cu(2) having small electronlike excess charge. As for O(1) configuration, (d) ordering is a better environment for hole transfer than (f). The metallic band originating from chain ordering, with its hybridization with apical atoms, is better suited to charge transfer than insulating disordered states.

Finally, the charge-transfer efficiency is the key to understand the PM-AF competition. Charge injection in the planes tends to stabilize the PM phase at increasing doping. At $x=0.5$, the AF-to-PM transition is accompanied by increase of $\simeq 0.05$ holes per CuO_2 unit for both the (d) or (f) configurations, i.e., the AF-PM hole charge imbalance does not depend on the O(1) configuration. This explains the substantial similarity of the two panels in Fig. 6.

In summary, we described from first principles the effects of oxygen doping in underdoped $YBa_2Cu_3O_{6+x}$. We found chain alignment energetically favored with respect to broken chains at any doping concentration. Since oxygen alignment ordering produces one-dimensional metallic bands, chain metallicity is formally present at any doping although over short distances only. We also considered the energy competition of the insulating AF and metallic PM states in the CuO_2 planes, showing that the latter phase is favored above a threshold doping located between $x=0.25$ and $x=0.5$. The in-plane AF-PM transition is caused by the (sparing) chain-to-plane hole transfer but is quite independent of the oxygen ordering in the chains.

This work was supported in part by MIUR through projects "Cervelli per la ricerca," PON-Cybersar, PRIN 2005, and by Fondazione Banco di Sardegna (Project Correlated oxides).

[1] G. Yu, C. H. Lee, D. Mihailovic, A. J. Heeger, C. Fincher, N. Herron, and E. M. McCarron, Phys. Rev. B **48**, 7545 (1993).
[2] Y.-S. Lee, K. Segawa, Y. Ando, and D. N. Basov, Phys. Rev. Lett. **94**, 137004 (2005).
[3] Y. Ando, K. Segawa, S. Komiya, and A. N. Lavrov, Phys. Rev. Lett. **88**, 137005 (2002).
[4] D. N. Basov, R. Liang, D. A. Bonn, W. N. Hardy, B. Dabrowski, M. Quijada, D. B. Tanner, J. P. Rice, D. M. Ginsberg, and T. Timusk, Phys. Rev. Lett. **74**, 598 (1995).
[5] K. Widder, J. Münzel, M. Göppert, D. Lüerßen, R. Becker, A. Dinger, H. P. Geserich, C. Klingshirn, M. Kläser, G. Müller-Vogt, J. Geerk, and V. M. Burlakov, Physica C **300**, 115 (1998).
[6] W. E. Pickett, Rev. Mod. Phys. **61**, 433 (1989); W. E. Pickett, R. E. Cohen, and H. Krakauer, Phys. Rev. B **42**, 8764 (1990).
[7] A. Filippetti and N. A. Spaldin, Phys. Rev. B **67**, 125109 (2003); **68**, 045111 (2003).
[8] B. Van Aken, T. T. M. Palstra, A. Filippetti, and N. A. Spaldin, Nature Mater. **3**, 164 (2004); A. Filippetti and V. Fiorentini, Phys. Rev. Lett. **95**, 086405 (2005); Phys. Rev. B **74**, 220401(R) (2006); Phys. Rev. Lett. **98**, 196403 (2007); Phys. Rev. B **77**, 235124 (2008).
[9] V. I. Anisimov, M. A. Korotin, J. Zaanen, and O. K. Andersen, Phys. Rev. Lett. **68**, 345 (1992).
[10] D. Vanderbilt, Phys. Rev. B **41**, 7892 (1990).
[11] G. Kresse and J. Furthmüller, Comput. Mater. Sci. **6**, 15 (1996); Phys. Rev. B **54**, 11169 (1996); G. Kresse and D. Joubert, *ibid.* **59**, 1758 (1999); The PAW potentials provided with VASP are used. The GGA is used by J. P. Perdew, J. A. Chevary, S. H. Vosko, K. A. Jackson, M. R. Pederson, D. J. Singh, and C. Fiolhais, *ibid.* **46**, 6671 (1992).
[12] C. Niedermayer, C. Bernhard, T. Blasius, A. Golnik, A. Moodenbaugh, and J. I. Budnick, Phys. Rev. Lett. **80**, 3843 (1998).